

# Sussex Research

## Time-dependent density functional study of the electronic potential energy curves and excitation spectrum of the oxygen molecule

Jingang Guan, Fan Wang, Tom Ziegler, Hazel Cox

### Publication date

01-01-2006

### Licence

This work is made available under the **Copyright not evaluated** licence and should only be used in accordance with that licence. For more information on the specific terms, consult the repository record for this item.

### Citation for this work (American Psychological Association 7th edition)

Guan, J., Wang, F., Ziegler, T., & Cox, H. (2006). *Time-dependent density functional study of the electronic potential energy curves and excitation spectrum of the oxygen molecule* (Version 1). University of Sussex. <https://hdl.handle.net/10779/uos.23310779.v1>

### Published in

Journal of Chemical Physics

### Link to external publisher version

<https://doi.org/10.1063/1.2217733>

### Copyright and reuse:

This work was downloaded from Sussex Research Open (SRO). This document is made available in line with publisher policy and may differ from the published version. Please cite the published version where possible. Copyright and all moral rights to the version of the paper presented here belong to the individual author(s) and/or other copyright owners unless otherwise stated. For more information on this work, SRO or to report an issue, you can contact the repository administrators at [sro@sussex.ac.uk](mailto:sro@sussex.ac.uk). Discover more of the University's research at <https://sussex.figshare.com/>

Guan, Jingang, Wang, Fan, Ziegler, Tom and Cox, Hazel

## Time-dependent density functional study of the electronic potential energy curves and excitation spectrum of the oxygen molecule

Article (Unspecified)

**Original citation:**

Guan, Jingang, Wang, Fan, Ziegler, Tom and Cox, Hazel (2006) Time-dependent density functional study of the electronic potential energy curves and excitation spectrum of the oxygen molecule. *Journal of Chemical Physics*, 125 (4). p. 44314. ISSN 0021-9606

This version is available from Sussex Research Online: <http://sro.sussex.ac.uk/583/>

This document is made available in accordance with publisher policies and may differ from the published version or from the version of record. If you wish to cite this item you are advised to consult the publisher's version. Please see the repository URL above for details on accessing the published version

**Copyright and reuse:**

Sussex Research Online is a digital repository of the research output of the University.

Copyright and all moral rights to the version of the paper presented here belong to the individual author(s) and/or other copyright owners. To the extent reasonable and practicable, the material made available in SRO has been checked for eligibility before being made available.

Copies of full text items generally can be reproduced, displayed or performed and given to third parties in any format or medium for personal research or study, educational, or not-for-profit purposes without prior permission or charge, provided that the authors, title and full bibliographic details are credited, a hyperlink and/or URL is given for the original metadata page and the content is not changed in any way.

# Time-dependent density functional study of the electronic potential energy curves and excitation spectrum of the oxygen molecule

Jingang Guan

*Department of Chemistry, School of Life Sciences, University of Sussex,  
Brighton BN1 9QJ, United Kingdom*

Fan Wang and Tom Ziegler

*Department of Chemistry, University of Calgary, Alberta T2N 1N4, Canada*

Hazel Cox<sup>a)</sup>

*Department of Chemistry, School of Life Sciences, University of Sussex,  
Brighton BN1 9QJ, United Kingdom*

(Received 27 February 2006; accepted 31 May 2006; published online 31 July 2006)

Orbital energies, ionization potentials, molecular constants, potential energy curves, and the excitation spectrum of O<sub>2</sub> are calculated using time-dependent density functional theory (TDDFT) with Tamm-Dancoff approximation (TDA). The calculated negative highest occupied molecular orbital energy ( $-\varepsilon_{\text{HOMO}}$ ) is compared with the energy difference ionization potential for five exchange correlation functionals consisting of the local density approximation (LDA<sub>xc</sub>), gradient corrected Becke exchange plus Perdew correlation (B<sub>88X</sub>+P<sub>86C</sub>), gradient regulated asymptotic correction (GRAC), statistical average of orbital potentials (SAOP), and van Leeuwen and Baerends asymptotically correct potential (LB94). The potential energy curves calculated using TDDFT with the TDA at internuclear distances from 1.0 to 1.8 Å are divided into three groups according to the electron configurations. The  $1\pi_u^4 1\pi_g^2$  electron configuration gives rise to the  $X^3\Sigma_g^-$ ,  $a^1\Delta_g$ , and  $b^1\Sigma_g^+$  states; the  $1\pi_u^3 1\pi_g^3$  electron configuration gives rise to the  $c^1\Sigma_u^-$ ,  $C^3\Delta_u$ , and  $A^3\Sigma_u^+$  states; and the  $B^3\Sigma_u^-$ ,  $A^1\Delta_u$ , and  $f^1\Sigma_u^+$  states are determined by the mixing of two or more electron configurations. The excitation spectrum of the oxygen molecule, calculated with the aforementioned exchange correlation functionals, shows that the results are quite sensitive to the choice of functional. The LDA<sub>xc</sub> and the B<sub>88X</sub>+P<sub>86C</sub> functionals produce similar spectroscopic patterns with a single strongly absorbing band positioned at 19.82 and 19.72 eV, respectively, while the asymptotically corrected exchange correlation functionals of the SAOP and the LB94 varieties yield similar excitation spectra where the computed strongly absorbing band is located at 16.09 and 16.42 eV, respectively. However, all of the exchange correlation functionals yield only one strongly absorbing band (oscillator strength greater than 0.1) in the energy interval of 0–20 eV, which is assigned to a  $X^3\Sigma_g^-$  to  $^3\Sigma_u^-$  transition. Furthermore, the oxygen molecule has a rich spectrum in the energy range of 14–20 eV and no spin allowed absorption bands are predicted to be observed in the range of 0–6 eV. © 2006 American Institute of Physics. [DOI: 10.1063/1.2217733]

## INTRODUCTION

The oxygen molecule plays an important role in human health, atmospheric photochemistry, and terrestrial chemistry. It is also one of the most abundant molecules in the Earth's atmosphere. Furthermore, the oxygen molecule is an interesting subject to many chemists, physicists, and aeronauts. Knowing the potential energy curve of the oxygen molecule, in various electronic states, should help in understanding its rich spectrum,<sup>1</sup> to calculate transport properties,<sup>2</sup> and to model the energy flow in the atmosphere of Earth and Venus.<sup>3</sup>

The six lowest bound electronic states of the oxygen molecule ( $X^3\Sigma_g^-$ ,  $a^1\Delta_g$ ,  $b^1\Sigma_g^+$ ,  $c^1\Sigma_u^-$ ,  $C^3\Delta_u$ , and  $A^3\Sigma_u^+$ ) possess long radiative lifetimes (from 150 ms for  $A^3\Sigma_u^+$  to 4000 s for  $a^1\Delta_g$ ). This metastability allows the oxygen mol-

ecule to provide a significant reservoir of energy in chemical reactions and photochemistry in the atmosphere, and at the same time, it greatly impedes the spectroscopic study of the oxygen molecule.<sup>4</sup> The  $a^1\Delta_g$  state of oxygen is important in biological chemistry and the  $b^1\Sigma_g^+$  state appears in afterglow, dayglow, nightglow, and in auroras.<sup>4</sup>

These six lowest bound electronic states have been studied experimentally and theoretically. Experimental characterization of these six bound states can be found in the literature.<sup>4,5</sup> Many theoretical calculations for these six bound states have also been published in the literature; Schaefer and Harris<sup>6</sup> as well as Beebe *et al.*<sup>7</sup> using configuration interaction (CI) method with minimum basis sets studied these six bound states and many other electronic states. Furthermore, Schaefer<sup>8</sup> using a larger basis set and an extensive CI method calculated the potential energy curve of the  $X^1\Sigma_u^-$  ground state. Moss and Goddard<sup>9</sup> employed the same method, but studied all the six bound states plus three extra

<sup>a)</sup>Electronic mail: h.cox@sussex.ac.uk

excited states. Later, Partridge *et al.*<sup>10</sup> using a multireference CI method obtained accurate results for the six bound states and their spectroscopic constants. Recently, Minaev and Minaeva<sup>1</sup> using an *ab initio* multiconfiguration self-consistent field (MCSCF) response method calculated potential energy curves of the six lowest bound states plus the double minima curves of the  $A^1\Delta_u$  and  $f^1\Sigma_u^+$  excited states as well as the important state  $B^3\Sigma_u^-$  which makes up the Schumann-Runge absorption band.<sup>5</sup> Whereas there are several studies of  $O_2$  using traditional *ab initio* CI and MCSCF methods, there is no study of these six lowest bound states with time-dependent density functional theory (TDDFT) in the literature. The present work uses the TDDFT method<sup>11–13</sup> for open shell molecular systems<sup>14–16</sup> at the Tamm-Dancoff approximation (TDA) level<sup>17</sup> and the spin-flip formalism published in the literature<sup>18,19</sup> to study the potential energy curves of the six lowest bound states, plus the important state of  $B^3\Sigma_u^-$  for the Schumann-Runge absorption and the two extra excited states  $A^1\Delta_u$  and  $f^1\Sigma_u^+$ . Spectroscopic constants for all of these electronic states and the excitation spectrum of the oxygen molecule are also presented here.

## METHODOLOGY AND COMPUTATIONAL DETAILS

Excitation energies,  $\omega$ , are calculated in TDDFT based on Eq. (1),<sup>11–13,20,21</sup>

$$\begin{pmatrix} \mathbf{A} & \mathbf{B} \\ \mathbf{B} & \mathbf{A} \end{pmatrix} \begin{pmatrix} X \\ Y \end{pmatrix} = \omega \begin{pmatrix} 1 & 0 \\ 0 & -1 \end{pmatrix} \begin{pmatrix} X \\ Y \end{pmatrix}, \quad (1)$$

where  $\mathbf{A}$  and  $\mathbf{B}$  are given as follows:

$$A_{ia,jb} = (\varepsilon_a - \varepsilon_i) \delta_{ij} \delta_{ab} + \left( \frac{\partial F_{ia}}{\partial P_{jb}} \right), \quad B_{ia,bj} = \left( \frac{\partial F_{ia}}{\partial P_{bj}} \right) \quad (2)$$

in terms of the Fock and density matrix elements  $F_{ia}$  and  $P_{jb}$ , respectively. In the above equations,  $i, j, \dots$  are indices used for occupied orbitals and  $a, b, \dots$  are indices for empty orbitals whereas  $p, q, \dots$  are indices for general orbitals. These orbitals are all unperturbed and calculated from a Kohn-Sham equation in the absence of a frequency dependent perturbation as

$$F\varphi_u = \varepsilon_u \varphi_u, \quad (3)$$

where

$$\begin{aligned} F(\hat{\rho})_{ia} &= F(\rho, s)_{ia} \\ &= \int \psi_i^* \left[ -\frac{1}{2} \nabla^2 + V_{Ne}(\mathbf{r}) + V_c(\rho) + V_{XC}(\rho, s) \right] \psi_a d\tau. \end{aligned} \quad (4)$$

We can assume without loss of generality that the unperturbed orbitals that are solutions to Eq. (3) are either  $\alpha$  or  $\beta$  orbitals and written in the two component representation as

$$\psi_p = \varphi_p^\alpha \alpha = \begin{pmatrix} \varphi_p^\alpha \\ 0 \end{pmatrix} \text{ and } \psi_q = \varphi_q^\beta \beta = \begin{pmatrix} 0 \\ \varphi_q^\beta \end{pmatrix}. \quad (5)$$

Thus the spin-density matrix due to the occupied unper-

turbed orbitals can be written in diagonal form without loss of generality as

$$\hat{\rho}^0 = \sum_i^{\text{occ}} \psi_i \psi_i^\dagger = \begin{pmatrix} \rho^{\alpha\alpha} & 0 \\ 0 & \rho^{\beta\beta} \end{pmatrix} = \frac{1}{2} \rho^0 \mathbf{I} + \frac{1}{2} [\rho^{\alpha\alpha} - \rho^{\beta\beta}] \sigma_z. \quad (6)$$

Here

$$\sigma_z = \begin{pmatrix} 1 & 0 \\ 0 & -1 \end{pmatrix} \quad (7)$$

is the Pauli  $z$  matrix, where

$$\rho^{\alpha\alpha} = \sum_i^{\text{occ}} \varphi_i^\alpha (\varphi_i^\alpha)^* \text{ and } \rho^{\beta\beta} = \sum_i^{\text{occ}} \varphi_i^\beta (\varphi_i^\beta)^*. \quad (8)$$

In the case where the spin-density matrix is diagonal the spin density can readily be defined as

$$s = \rho^{\alpha\alpha} - \rho^{\beta\beta}. \quad (9)$$

The matrices  $\mathbf{A}$  and  $\mathbf{B}$  are according to Eq. (2) defined in terms of

$$\frac{\delta F_{ia}}{\delta P_{jb}} = \left( \frac{F(\hat{\rho})_{ia} - F(\hat{\rho}^0)_{ia}}{\Delta P_{jb}} \right)_{(\Delta P_{jb}=0)}, \quad (10)$$

where  $\hat{\rho}^0$  is the unperturbed spin-density matrix of Eq. (6) and

$$\hat{\rho} = \hat{\rho}^0 + \Delta P_{jb} \psi_j \psi_b^\dagger. \quad (11)$$

In the case where  $j$  and  $b$  are of the same spin both  $\hat{\rho}$  and  $\hat{\rho}^0$  are diagonal. Thus,  $F(\hat{\rho})_{ia}$  as well as  $F(\hat{\rho}^0)_{ia}$  are readily evaluated based on the regular collinear expression for the exchange correlation potential,

$$\begin{pmatrix} V_{XC}^{\alpha\alpha} & 0 \\ 0 & V_{XC}^{\beta\beta} \end{pmatrix} = \frac{\delta E_{XC}[\rho, s]}{\delta \rho} \mathbf{I} + \frac{\delta E_{XC}[\rho, s]}{\delta |s|} \frac{s \sigma_z}{|s|}. \quad (12)$$

We obtain the expression

$$\begin{aligned} \frac{\partial F_{ia}}{\partial P_{jb}} = & \int \psi_i^*(\mathbf{r}_1) \psi_a(\mathbf{r}_1) \psi_j^*(\mathbf{r}_2) \psi_b(\mathbf{r}_2) \frac{1}{|\mathbf{r}_1 - \mathbf{r}_2|} d\tau_1 d\tau_2 + \int (\psi_j^* \psi_b) (\psi_i^* \psi_a) \frac{\delta^2 E_{XC}}{\partial \rho^2} d\tau + \int [(\psi_j^* \sigma_z \psi_b) (\psi_i^* \psi_a) + (\psi_j^* \psi_b) \\ & \times (\psi_i^* \sigma_z \psi_a)] \frac{m_z}{s} \frac{\delta^2 E_{XC}}{\partial \rho \partial s} d\tau + \int (\psi_j^* \sigma_z \psi_b) (\psi_i^* \sigma_z \psi_a) \frac{\delta^2 E_{XC}}{\partial s^2} d\tau \end{aligned} \quad (13)$$

that is nonzero provided that  $i$  has the same spin as  $a$  and  $j$  the same spin as  $b$ .

On the other hand if  $j$  and  $b$  are of different spins, then the spin-density matrix  $\hat{\rho}$  of Eq. (11) is nondiagonal. In this case Eq. (12) does not apply.<sup>22-24</sup> However, we can perform a unitary transformation

$$\begin{pmatrix} \alpha' \\ \beta' \end{pmatrix} = U \begin{pmatrix} \alpha \\ \beta \end{pmatrix} \quad (14)$$

such that the density matrix  $\hat{\rho}$  becomes diagonal,

$$\begin{aligned} U^\dagger \begin{pmatrix} \rho^{\alpha\alpha} & \rho^{\beta\alpha} \\ \rho^{\alpha\beta} & \rho^{\beta\beta} \end{pmatrix} U &= \begin{pmatrix} \rho^{\alpha'\alpha'} & 0 \\ 0 & \rho^{\beta'\beta'} \end{pmatrix} \\ &= \frac{1}{2} \rho \mathbf{I} + \frac{1}{2} [\rho^{\alpha'\alpha'} - \rho^{\beta'\beta'}] \sigma_z, \end{aligned} \quad (15)$$

where  $s' = \rho^{\alpha'\alpha'} - \rho^{\beta'\beta'}$  is the new spin density. In this representation we are able to make use of the collinear exchange correlation potential given by

$$\begin{pmatrix} V_{XC}^{\alpha'\alpha'} & 0 \\ 0 & V_{XC}^{\beta'\beta'} \end{pmatrix} = \frac{\delta E_{XC}[\rho, s']}{\delta \rho} \mathbf{I} + \frac{\delta E_{XC}[\rho, s']}{\delta |s'|} \frac{s' \sigma_z}{|s'|}. \quad (16)$$

We can finally obtain an expression for the exchange correlation potential in the original nondiagonal  $(\alpha, \beta)$  representation by applying a unitary back-transformation on both sides of Eq. (16) to obtain

$$\begin{aligned} U \begin{pmatrix} V_{XC}^{\alpha'\alpha'} & 0 \\ 0 & V_{XC}^{\beta'\beta'} \end{pmatrix} U^\dagger &= \begin{pmatrix} V_{XC}^{\alpha\alpha} & V_{XC}^{\alpha\beta} \\ V_{XC}^{\beta\alpha} & V_{XC}^{\beta\beta} \end{pmatrix} \\ &= \frac{\delta E_{XC}[\rho, s']}{\delta \rho} \mathbf{I} \\ &\quad + \frac{\delta E_{XC}[\rho, s']}{\delta |s'|} \frac{U(s' \sigma_z) U^\dagger}{|s'|}. \end{aligned} \quad (17)$$

After some manipulations<sup>25</sup> one can express the right hand side of Eq. (17) in terms that are completely defined in the nondiagonal  $(\alpha, \beta)$  representation. Thus,

$$\begin{pmatrix} V_{XC}^{\alpha\alpha} & V_{XC}^{\alpha\beta} \\ V_{XC}^{\beta\alpha} & V_{XC}^{\beta\beta} \end{pmatrix} = \frac{\delta E_{XC}[\rho, |m|]}{\delta \rho} \mathbf{I} + \frac{\delta E_{XC}[\rho, |m|]}{\delta |m|} \frac{\mathbf{m} \cdot \boldsymbol{\sigma}}{|m|}. \quad (18)$$

Here

$$\sigma_x = \begin{pmatrix} 0 & 1 \\ 1 & 0 \end{pmatrix} \text{ and } \sigma_y = \begin{pmatrix} 0 & -i \\ i & 0 \end{pmatrix} \quad (19)$$

and

$$[\rho^{\alpha\beta} + \rho^{\beta\alpha}] = \sum_i^{\text{occ}} \psi_i^* \sigma_x \psi_i = m_x, \quad (20a)$$

$$i[-\rho^{\alpha\beta} + \rho^{\beta\alpha}] = \sum_i^{\text{occ}} \psi_i^* \sigma_y \psi_i = m_y, \quad (20b)$$

$$[\rho^{\alpha\alpha} - \rho^{\beta\beta}] = \sum_i^{\text{occ}} \psi_i^* \sigma_z \psi_i = m_z. \quad (20c)$$

The expression given in Eq. (18) is referred to as the non-collinear formulation for the exchange correlation potential. It deals with the relativistic limit where the spin-orbit operator can mix orbitals of different spins. However, we have shown<sup>17,18,24</sup> that it also is the formulation of choice in the nonrelativistic limit where a perturbation such as a spin flip mixes orbitals of different spins. Recently, a TDDFT formalism based on the noncollinear exchange correlation functional of Eq. (18) was published in the literature<sup>18,19</sup> to deal with spin-flip transitions. In the spin-flip transition case, the derivative  $\partial F_{ia} / \partial P_{jb}$  is written as

$$\begin{aligned} \frac{\partial F_{ia}}{\partial P_{jb}} = & \int (\psi_j^* \sigma_x \psi_b) (\psi_i^* \sigma_x \psi_a) \frac{1}{s} \frac{\delta E_{XC}}{\delta s} d\tau \\ & + \int (\psi_j^* \sigma_y \psi_b) (\psi_i^* \sigma_y \psi_a) \frac{1}{s} \frac{\delta E_{XC}}{\delta s} d\tau. \end{aligned} \quad (21)$$

Here  $i, a$  should be of different spin as should  $j, b$ . We shall in the following make extensive use of Eq. (21) and the newly implemented spin-flip TDDFT method.<sup>18,19</sup>

If the TDA (Ref. 17) is used, Eq. (1) for calculating excitation energies can be simplified as

$$AX = \omega X.$$

All of the present calculations are performed using TDDFT with TDA approximation, which is referred to as TDDFT/TDA.

To calculate excitation energies using the Amsterdam density functional<sup>26-29</sup> (ADF) program, first a SCF calculation is performed to obtain the orbitals and orbital energies. Different exchange correlation functionals were used in this step. Next, excitation energies are calculated as a post SCF step using the adiabatic local density approximation (ALDAxc).<sup>30</sup> The five exchange correlation functionals tested in the SCF step were the local density approximation<sup>31</sup> (LDAxc), Becke exchange<sup>32</sup> plus Perdew correlation<sup>33</sup> (B88x+P86c), gradient regulated asymptotic correction (GRAC),<sup>34</sup> statistical average of orbital potentials (SAOP),<sup>35</sup> and van Leeuwen and Baerends asymptotically correct ex-



TABLE I. Vertical excitation energies (eV) calculated with the LDAxc exchange correlation functional and different qualities of basis sets.

O <sub>2</sub>	<sup>1</sup> Δ <sub>g</sub>	<sup>1</sup> Σ <sub>g</sub> <sup>+</sup>	<sup>1</sup> Σ <sub>u</sub> <sup>-</sup>	<sup>1</sup> Δ <sub>u</sub>	<sup>3</sup> Δ <sub>u</sub>	<sup>3</sup> Σ <sub>u</sub> <sup>+</sup>	<sup>3</sup> Π <sub>g</sub>	<sup>3</sup> Σ <sub>u</sub> <sup>-</sup>
TZ2P	1.05	2.06	7.11	8.02	7.03	7.17	7.94	9.33
ET-QZ3P	1.06	2.07	7.11	8.02	7.03	7.17	7.96	9.30
ET-QZ3P-1Diffuse	1.06	2.06	7.07	8.00	7.02	7.16	7.18	8.40
ET-QZ3P-2Diffuse	1.06	2.06	7.01	7.26	7.04	7.16	6.57	7.19
ET-QZ3P-3Diffuse	1.06	2.06	6.85	6.88	6.85	6.88	6.60	6.87

change correlation potential<sup>36</sup> (LB94). Finally, the LB94 exchange correlation functional is chosen for computing the potential energy curves, molecular spectroscopic constants, and the excitation spectrum of the oxygen molecule. In the post SCF step, the ALDAxc (Ref. 37) was utilized for the exchange correlation kernel for all of the calculations, hence only the exchange correlation functional used in the SCF step will be used as reference in this paper. The ground state potential energy curve was calculated with the LDAxc functional. The excited state potential energy curves were obtained by combining the LDAxc ground state energies and the LB94 excitation energies.

The basis set used in the present calculations is the even-tempered quadruple zeta plus three polarization functions and three diffuse functions (ET-QZ3P-3Diffuse) in the ADF basis set library. However, the effect of basis set on the excitation energies was assessed and will be presented in the next section. All of the convergence criteria used are the ADF default values, except the integration accuracy parameter, which is set to 6.

## RESULTS AND DISCUSSION

In order to evaluate the quality of the basis used for further excitation energy calculations, the lowest eight excitation energies for the first excited state of each symmetry of the oxygen molecule have been calculated at the experimental bond length (1.2075 Å),<sup>38</sup> using the LDAxc exchange correlation functional with different qualities of basis sets (see Table I). The results in Table I show that the excitation energy calculations with a spin flip are less sensitive to the choice of the basis set. For example, excitation energies to the singlet excited states of <sup>1</sup>Δ<sub>g</sub> and <sup>1</sup>Σ<sub>g</sub><sup>+</sup> do not change when the quality of the basis set is increased from the TZ2P to the highest quality basis of ET-QZ3P-3Diffuse. However, spin-preserved electronic transitions from the highest occupied molecular orbital (HOMO) to the lowest unoccupied molecular orbital (LUMO) demand higher quality basis sets, e.g., the excitation energy to the triplet excited state <sup>3</sup>Π<sub>g</sub>(1π<sub>g</sub> → 4σ<sub>g</sub>) changed by 0.61 eV by adding a second diffuse function to the ET-QZ3P-1Diffuse basis, whereas the highest quality basis, the ET-QZ3P-3Diffuse, has little improvement on the excitation energy, which is only changed by about 0.03 eV, and appears reasonably converged. While other kinds of transitions demand even higher quality of basis set, such as the triplet <sup>3</sup>Σ<sub>u</sub><sup>-</sup> excited state, corresponding to the electron transition 1π<sub>g</sub> → 2π<sub>u</sub>, its excitation energy changes by 0.32 eV from ET-QZ3P-2Diffuse basis to ET-QZ3P-3Diffuse basis. Since the ET-QZ3P-3Diffuse is the highest

quality basis set for oxygen in the ADF program basis library and the excitation spectrum of the oxygen molecule involves many

Rydberg transitions, the ET-QZ3P-3Diffuse basis has to be used in the present calculations.

Orbital energies of the oxygen molecule calculated with ET-QZ3P-3Diffuse basis set and using LDAxc, B<sub>88X</sub>+P<sub>86C</sub>, GRAC, SAOP, and LB94 exchange correlation functionals are given in Table II. It can be seen from Table II that the LDAxc, the B<sub>88X</sub>+P<sub>86C</sub>, the GRAC, and the SAOP functionals produce the same ground state electron configuration, which is as

$$1\sigma_g^2 1\sigma_u^2 2\sigma_g^2 2\sigma_u^2 3\sigma_g^2 1\pi_u^4 1\pi_g^2.$$

But the LB94 functional predicted that the 1π<sub>u</sub> orbital energy is lower than the 3σ<sub>g</sub> orbital energy, which is contrary to the other functionals. However, this is due to the basis set used, as the orbital ordering of the ground state electron configuration can be corrected by using a “special diffuse” basis set, which contains triple zeta functions for the valence electrons plus one 3p, two 3d, one 4s, and one 4f functions, labeled as O.1s.spd in the ADF basis library. Using this very diffuse O.1s.spd basis, the LB94 functional gives the same level ordering of the ground state as the other four functionals and is in agreement with the electron configuration of the oxygen molecule in the literature.<sup>1,6</sup> The ground state electron configuration is simply written as 1π<sub>u</sub><sup>4</sup>1π<sub>g</sub><sup>2</sup>. It is noticed from Table II that the orbital energies are less stable in the calculations of the LDAxc, the B<sub>88X</sub>+P<sub>86C</sub>, and the GRAC functionals compared to those computed by the SAOP and the LB94 functionals. In fact, the GRAC functional produces no bound virtual orbitals, while the LDAxc and the B<sub>88X</sub>+P<sub>86C</sub> functionals produce only three bound unoccupied orbitals. The SAOP and the LB94 functionals yield six and seven bound virtual orbitals, respectively. However, the previous Hartree-Fock (HF) calculations in the literature,<sup>39</sup> although giving a reasonably stable HOMO, gave no bound virtual orbital. This is to be expected since virtual HF orbitals see one electron more than occupied HF orbitals.<sup>40</sup>

On the other hand, DFT virtual and occupied orbitals see the same number of electrons. According to fundamental DFT theory<sup>41</sup> (Koopmans’ theorem is for HF), the negative of the HOMO energy is equal to the ionization potential (IP) energy, if the exchange correlation functional is exact. In practice, the IP derived from this Koopmans-type theorem is not usually the same as the IP calculated from the energy difference of the neutral and the cation species. This is due to approximations used in the exchange correlation functionals

TABLE II. Orbital energies and energy difference IPs of the oxygen molecule calculated with an ET-QZ3P-3Diffuse basis and different exchange correlation functionals based on  $\alpha$  electron orbital energies: the unit is in electron volts (eV). The experimental IP=12.1 eV was taken from Ref. 42.

Orbital	DFT					HF <sup>a</sup>
	LDAxc (IP=12.75)	B <sub>88X</sub> +P <sub>86C</sub> (IP=12.74)	GRAC (IP=12.74)	SAOP (IP=12.25)	LB94 (IP=13.25)	
1 $\sigma_g$	-510.672	-514.937	-514.805	-519.864	-539.541	-564.446
1 $\sigma_u$	-510.669	-514.935	-514.803	-519.862	-539.539	-564.419
2 $\sigma_g$	-32.940	-32.994	-32.903	-37.930	-38.541	-45.035
2 $\sigma_u$	-20.288	-20.605	-20.520	-26.023	-26.490	-29.933
3 $\sigma_g$	-13.837	-13.659	-13.555	-18.837	-19.903	-19.837
1 $\pi_u$	-13.717	-13.655	-13.552	-18.837	-19.927	-19.238
1 $\pi_g$ (HOMO)	-6.897	-6.937	-6.822	-12.268	-13.273	-14.531
4 $\sigma_g$ (LUMO)	-0.277	-0.349	3.479	-3.382	-3.975	0.490
3 $\sigma_u$	-0.045	-0.177	3.315	-2.855	-3.781	0.898
4 $\sigma_u$	0.154	0.033	6.139	-0.633	-1.590	2.857
5 $\sigma_g$	0.153	0.040	6.778	-0.542	-1.155	3.048
5 $\sigma_u$	0.618	0.531	8.026	0.928	-0.350	3.374
2 $\pi_u$	-0.017	-0.055	5.265	-1.950	-2.464	0.871
2 $\pi_g$	0.182	0.137	7.189	-0.544	-0.839	1.143

<sup>a</sup>Reference 39.

<sup>b</sup>The LUMO calculated by the GRAC functional is 3 $\sigma_u$ .

and relaxation around the hole. Table II shows that Koopmans' IPs computed using the LDAxc, the B<sub>88X</sub>+P<sub>86C</sub>, and the GRAC functionals are 6.90, 6.94, and 6.82 eV, respectively, which are much lower than the energy difference IPs calculated using the same functionals (12.75 eV for the LDAxc and 12.74 eV for both the B<sub>88X</sub>+P<sub>86C</sub> and the GRAC) and experimental result (12.1 eV).<sup>42</sup> This indicates that these exchange correlation functionals underestimate the HOMO orbital energy due to the fact that they do not have correct asymptotic behavior, except for the GRAC functional. While the asymptotically correct exchange correlation functionals of the SAOP and the LB94 calculated Koopmans' IPs (12.27 eV for the SAOP and 13.27 eV for the LB94) are very close to energy difference IPs computed by the same functionals (12.25 eV for the SAOP and 13.25 eV for the LB94), the difference between the two calculations of IP is only 0.02 eV for both the SAOP and the LB94 functionals. Furthermore, the calculated energy difference IP using either the SAOP or the LB94 functionals is comparable with experiment (12.1 eV);<sup>42</sup> the deviations are 0.15 and 1.15 eV, respectively. The present Koopmans-type IP calculated from the SAOP functional agree well with a previous exact exchange potential DFT calculated Koopmans' IP of 12.9 eV by Veseth<sup>39</sup> with a deviation of 0.63 eV, but Koopmans' IP calculated by the LB94 functional agree well with the exact local exchange potential DFT Koopmans' IP calculation of 13.6 eV by Görling<sup>42</sup> with a deviation of 0.33 eV. This indicates that the SAOP and the LB94 functionals produce better HOMO orbital energies than the LDAxc, the B<sub>88X</sub>+P<sub>86C</sub>, and the GRAC functionals. In addition, the HOMO and LUMO orbital energy differences calculated by the LDAxc functional (6.62 eV) and the B<sub>88X</sub>+P<sub>86C</sub> functional (6.59 eV) are much smaller than those computed by the SAOP functional (8.89 eV) and the LB94 functional (9.30 eV). However, the GRAC functional, which yields dif-

ferent LUMO orbital (3 $\sigma_u$ ) from the other functionals (4 $\sigma_g$ ), gives the largest HOMO and LUMO orbital energy gap (10.14 eV). Since different exchange correlation functionals give different orbital energies and orbital energy gaps, and orbital energies are an important ingredient in the calculations of excitation energies using TDDFT/TDA method, further evaluation of different exchange correlation functionals in excitation energy calculations is required.

Exchange correlation functionals are further evaluated in excitation energy calculations of oxygen molecule by comparing with available experimental results and other theoretical calculations. The excitation energies of the oxygen molecule calculated with ET-QZ3P-3Diffuse basis using the LDAxc, the B<sub>88X</sub>+P<sub>86C</sub>, the GRAC, the SAOP, and the LB94 functionals are given in Table III. This table shows that the exchange correlation functional has a dramatic impact on the excitation energies, which can vary by as much as 3 eV with different functionals. For example, the excitation energy for the  $^3\Sigma_u^-$  state differs by 3.24 eV between LDAxc and GRAC. It is noticed that the excitation energies calculated by the LDAxc and the B<sub>88X</sub>+P<sub>86C</sub> functionals are very similar; the excitation energies computed by the two functionals differ by 0.00–0.32 eV. While the asymptotically corrected SAOP and LB94 functionals also yield similar excitation energies, the differences between the SAOP and the LB94 calculated excitation energies are 0.01–0.40 eV. However, the GRAC functional always gives the largest excitation energies for the listed excited states. Overall, excitation energies computed using the LB94 functional are closest to the experimental results and previous theoretical calculations. The deviations between the LB94 functional calculated excitation energies and experiment<sup>5</sup> are 0.15 and 0.23 eV for the singlet excited states of  $^1\Sigma_g^+$  and  $^1\Delta_g$ . For the triplet excited states  $^3\Sigma_u^+$  and the  $^3\Sigma_u^-$ , the excitation energies calculated with the LB94 functional are about 0.78 and 1.03 eV larger than experi-

TABLE III. Vertical excitation energies of the oxygen molecule calculated with an ET-QZ3P-3Diffuse basis and different exchange correlation functionals in comparison with experiment and previous theoretical results.

Methods and functionals	$^1\Delta_g$	$^1\Sigma_g^+$	$^1\Sigma_u^-$	$^1\Delta_u$	$^3\Delta_u$	$^3\Sigma_u^+$	$^3\Pi_g$	$^3\Sigma_u^-$
LDAXc	1.06	2.06	7.08	6.88	6.87	6.88	6.60	6.87
B <sub>88</sub> X+P <sub>86</sub> C	1.37	2.38	6.90	6.90	6.87	6.88	6.57	6.89
GRAC	1.34	2.34	7.22	8.05	7.085	7.18	8.35	10.11
SAOP	1.13	2.15	6.91	7.83	6.98	7.07	7.97	9.64
LB94	0.76	1.79	6.62	7.56	6.68	6.78	7.57	9.63
HF <sup>a</sup>	0.85	1.36	5.22		5.37	5.52	7.80	10.53
CI <sup>a</sup>	1.13	1.86	6.25		6.50	6.66	8.33	9.11
Coupled Cluster <sup>b</sup>					6.25	6.41	8.04	9.31
Expt. <sup>c</sup>	0.99	1.64				$\sim 6^d$		$8.6^d$

<sup>a</sup>Reference 39.<sup>c</sup>Reference 5.<sup>b</sup>Reference 43.<sup>d</sup>Reference 9.

ment. That is 0.12 and 0.52 eV higher than those computed by the CI method, and about 0.37 and 0.32 eV larger than the excitation energies calculated by coupled cluster method.<sup>43</sup>

Comparison of experimental potential energy curves of the six lowest bound states ( $X^3\Sigma_g^-$ ,  $a^1\Delta_g$ ,  $b^1\Sigma_g^+$ ,  $c^1\Sigma_u^-$ ,  $C^3\Delta_u$ , and  $A^3\Sigma_u^+$ ) of the O<sub>2</sub> molecule with the LB94 functional and the ET-QZ3P-3Diffuse basis calculations within the internuclear distances from 1.0 to 1.8 Å are given in Fig. 1. In addition, the important  $B^3\Sigma_u^-$  state due to the Schumann-Runge absorption, the  $A^1\Delta_u$  excited state, and the  $f^1\Sigma_u^+$  excited state potential energy curves are also shown in Fig. 1. The lowest three potential energy curves due to the  $X^3\Sigma_g^-$ , the  $a^1\Delta_g$ , and the  $b^1\Sigma_g^+$  electronic states have similar shapes and no crossing among them. These shapes are in basic agreement with experimental results,<sup>5</sup> especially the repulsive part of the curves at the small internuclear distance region (1.0–1.3 Å). However, significant deviations between the experimental and the calculated curves can be observed at larger internuclear distance. In fact, the dissociation limit is considerably overestimated by about 2.6 eV. The difference appears at smaller distance for the higher excited state

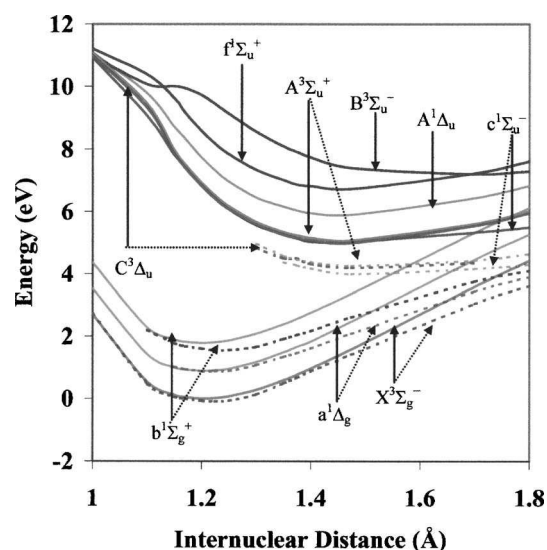


FIG. 1. Potential energy curves of the oxygen molecule calculated with the LB94 exchange correlation functional (solid lines) compared with experimental curves (Ref. 5) (dashed lines).

curves. For the ground state of  $X^3\Sigma_g^-$ , a difference of about 0.18 eV occurs at the internuclear distance 1.5 Å. For the excited state of  $a^1\Delta_g$ , the difference becomes obvious (0.20 eV) at the internuclear distance of 1.4 Å. For the higher excited state of  $b^1\Sigma_g^+$ , the difference can be observed (0.20 eV) at the internuclear distance of 1.2 Å. The potential energy curves of the second group of excited states,  $c^1\Sigma_u^-$ , the  $C^3\Delta_u$ , and  $A^3\Sigma_u^+$ , also have similar shapes and are closely distributed in the nuclear distance interval of 1.0–1.8 Å (the  $c^1\Sigma_u^-$  at the bottom, the  $C^3\Delta_u$  in the middle, and the  $A^3\Sigma_u^+$  on top), which is in qualitative agreement with experiment.<sup>5</sup> However, the calculated excited state curves need to be downshifted by about 1.0 eV to overlap with the experimental curves. The other excited state potential energy curves of  $B^3\Sigma_u^-$ ,  $A^1\Delta_u$ , and  $f^1\Sigma_u^+$  are quite different. The similarity of the potential energy curves of the electronic states within the first group ( $X^3\Sigma_g^-$ ,  $a^1\Delta_g$ , and  $b^1\Sigma_g^+$ ) and within the second group ( $c^1\Sigma_u^-$ ,  $C^3\Delta_u$ , and  $A^3\Sigma_u^+$ ) is attributed to the fact that the states in each group are described by the same electron configuration. Thus, the first group,  $X^3\Sigma_g^-$ ,  $a^1\Delta_g$ , and  $b^1\Sigma_g^+$ , is characterized by the electron configuration  $1\pi_u^4 1\pi_g^2$  (100%), while the second group,  $c^1\Sigma_u^-$ ,  $C^3\Delta_u$ , and  $A^3\Sigma_u^+$ , is determined by the electron configuration  $1\pi_u^3 1\pi_g^3$  (100%). The  $B^3\Sigma_u^-$  excited state potential energy curve obtained by the present TDDFT/TDA calculations is different from other excited states, in that it has a double minima. This double minima state may be caused by the mixing of a few electron configurations [ $1\pi_u^3 1\pi_g^3$  (59.5%),  $1\pi_u^4 1\pi_g^2 2\pi_u^1$  (29.3%), and  $3a_{1g}^1 \pi_u^4 1\pi_g^2 3a_{2u}^1$  (2.5%)]. Although curves with double minima were observed in the MCSCF calculations,<sup>1</sup> these were found for the  $A^1\Delta_u$  and the  $f^1\Sigma_u^+$  excited states.

The equilibrium distances, vibrational frequencies, and transition energies corresponding to the different states of the oxygen molecule were calculated with the ET-QZ3P-3Diffuse basis using the LB94 functional and the results are listed in Table IV. It can be seen from this table that the electronic states  $X^3\Sigma_g^-$ ,  $a^1\Delta_g$ , and  $b^1\Sigma_g^+$  due to the electron configuration  $1\pi_u^4 1\pi_g^2$  have equilibrium bond distances in the narrow range from 1.201 Å ( $b^1\Sigma_g^+$ ) to 1.203 Å ( $X^3\Sigma_g^-$  and  $a^1\Delta_g$ ), which agree well with the range of experimental bond lengths<sup>5</sup> of 1.208 Å ( $X^3\Sigma_g^-$ ), 1.216 Å ( $a^1\Delta_g$ ), and



TABLE IV. Molecular constants for eight bound states of the oxygen molecule calculated with the LB94 exchange correlation functional.

State	Method	$r_e$ (Å)	$\omega_e$ (cm <sup>-1</sup> )	$T_e$ (eV)
$X^3\Sigma_g^-$	Present work	1.203	1621.0	
	CI <sup>a</sup>	1.236	1498.8	
	MRCI <sup>b</sup>	1.210	1558	
	GVB+CI <sup>c</sup>	1.238	1692.7	
	Expt. <sup>d</sup>	1.208	1580.2	
$a^1\Delta_g$	Present work	1.203	1623.3	0.891
	CI <sup>a</sup>	1.250	1403.4	1.098
	MRCI <sup>b</sup>	1.219	1501	0.964
	GVB+CI <sup>c</sup>	1.249	1595.0	1.089
	Expt. <sup>d</sup>	1.216	1509.3	0.982
$b^1\Sigma_g^+$	Present work	1.201	1605.5	1.793
	CI <sup>a</sup>	1.267	1310.8	1.776
	MRCI <sup>b</sup>	1.231	1446	1.652
	GVB+CI <sup>c</sup>	1.260	1505.1	1.691
	Expt. <sup>d</sup>	1.227	1432.7	1.636
$c^1\Sigma_u^+$	Present work	1.434	1121.0	5.030
	CI <sup>d</sup>	1.555	759.8	3.888
	MRCI <sup>b</sup>	1.521	754	
	GVB+CI <sup>c</sup>	1.525	832.6	3.937
	Expt. <sup>d</sup>	1.517	794.3	4.098
$C^3\Delta_u$	Present work	1.542	1098.2	4.901
	CI <sup>a</sup>	1.550	780.1	4.130
	MRCI <sup>b</sup>	1.517	770	
	GVB+CI <sup>c</sup>	1.522	858.6	4.173
	Expt. <sup>d</sup>	~1.5	750	4.306
$A^3\Sigma_u^+$	Present work	1.546	1139.7	4.966
	CI <sup>a</sup>	1.558	764.6	4.206
	MRCI <sup>b</sup>	1.524	765	
	GVB+CI <sup>c</sup>	1.528	836.6	4.249
	Expt. <sup>d</sup>	1.522	799.1	4.389
$1^1\Delta_u$	Present work	1.458	946.3	5.898
	CI <sup>a</sup>	1.631	705.6	8.570
	GVB+CI <sup>c</sup>	1.648	627.2	8.794
	Expt. <sup>e</sup>	~1.6		
$f^1\Sigma_u^+$	Present work	1.467	931.1	6.733
	CI <sup>a</sup>	1.611	792.4	10.430
	GVB+CI <sup>c</sup>	1.655	652.8	10.187
	Expt. <sup>e</sup>	1.622		

<sup>a</sup>Reference 45.<sup>b</sup>Reference 10.<sup>c</sup>Reference 9.<sup>d</sup>Reference 5.<sup>e</sup>Reference 46.

1.227 Å ( $b^1\Sigma_g^+$ ). Transition energies of the previous two excited states ( $a^1\Delta_g$  and  $b^1\Sigma_g^+$ ) are 0.891 and 1.793 eV with deviations of 0.091 and -0.140 eV, respectively, relative to experiment.<sup>5</sup> They are close to those obtained by multiple reference configuration interaction (MRCI) calculations.<sup>10</sup> The excited states  $c^1\Sigma_u^-$ ,  $C^3\Delta_u$ , and  $A^3\Sigma_u^+$  due to the electron configuration  $1\pi_u^3 1\pi_g^3$  have larger equilibrium nuclear distances which are in the range of 1.434–1.546 Å; the deviations from experiment<sup>5</sup> are 0.024–0.083 Å. Transition energies of 5.030, 4.901, and 4.966 eV for the  $c^1\Sigma_u^-$ , the  $C^3\Delta_u$ , and the  $A^3\Sigma_u^+$  excited states have deviations of -0.932, -0.674, and -0.714 eV, respectively, compared to experi-

mental results. The highest lying excited states  $1^1\Delta_u$  and  $f^1\Sigma_u^+$  have bond lengths of 1.458 and 1.467 Å, respectively. These values are about 0.150 Å shorter than those observed experimentally.<sup>5</sup>

Excitation spectra of the oxygen molecule calculated with the LDAxc, the B<sub>88</sub>X+P<sub>86</sub>C, the GRAC, the SAOP, and the LB94 exchange correlation functionals are given in Figs. 2–6, respectively. The ionization threshold, the negative HOMO orbital energy ( $-\epsilon_{\text{HOMO}}$ ), corresponding to each functional is also given in the figures. The excitation spectra of the O<sub>2</sub> in Figs. 2–6 show that the oxygen molecule has no spin allowed absorptions below 6 eV and possesses rich

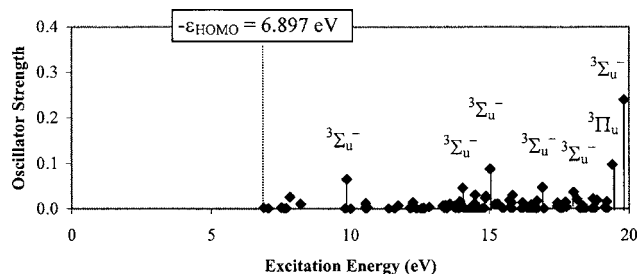


FIG. 2. Excitation spectrum of the oxygen molecule calculated with the LDAxc exchange correlation functional.

spectrum in the energy interval between 14 and 20 eV, which is above the corresponding ionization threshold ( $-\epsilon_{\text{HOMO}}$ ) and in the ionization continuum region. However, a few excitation peaks occur below the ionization threshold for the asymptotically corrected functionals of SAOP and LB94, since the asymptotically corrected SAOP and LB94 functionals produce a larger ionization threshold than the other three functionals as seen in the orbital energy discussion at the beginning of this section. It is noted that the choice of exchange correlation functional strongly influences the position of the predicted absorption lines due to the spectra lying in the ionization continuum region. The LDAxc and the B<sub>88</sub>X+P<sub>86</sub>C functionals give rise to very similar spectroscopic pattern; both functionals produce one strong absorption band and six peaks of medium intensity. The strong absorption bands predicted by these two functionals are positioned very closed to each other; the envelope peaking is at 19.82 and 19.72 eV, respectively. The asymptotically corrected exchange correlation functionals of the SAOP and LB94 variety also yield similar absorption spectra with one strong band and eight peaks of medium intensity. The locations of the strong band are at 16.09 and 16.42 eV, respectively, for the SAOP and the LB94 functionals. The GRAC functional also produces one strong band and eight medium peaks, but the strong band is now located at 18.61 eV. The strong band predicted by the five aforementioned functionals is in all cases assigned to the  $^3\Sigma_u^-$  excited state, but corresponds to different orbital transitions. The strong absorption band predicted by the LDAxc functional corresponds to Rydberg orbital transitions of the following types:  $2\sigma_{2u} \rightarrow 8\sigma_{1g}(\beta, 24\%)$ ,  $2\sigma_{2u} \rightarrow 4\sigma_{1g}(\alpha, 19\%)$ ,  $3\sigma_{1g} \rightarrow 10\sigma_{2u}(\alpha, 14\%)$ , and  $3\sigma_{1g} \rightarrow 10\sigma_{2u}(\beta, 12\%)$ . In the case of the B<sub>88</sub>X+P<sub>86</sub>C functional, the strong band originates from the Rydberg orbital transition  $1\pi_{1u} \rightarrow 3\pi_{2g}(\beta, 99\%)$ , whereas

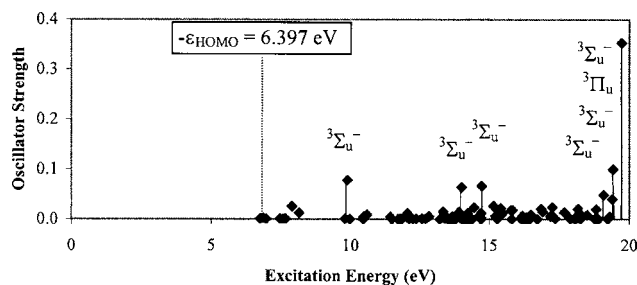


FIG. 3. Excitation spectrum of the oxygen molecule calculated with the B<sub>88</sub>X+P<sub>86</sub>C exchange correlation functional.

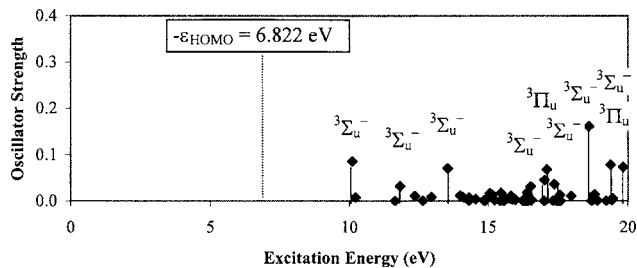


FIG. 4. Excitation spectrum of the oxygen molecule calculated with the GRAC exchange correlation functional.

excitations to  $^3\Sigma_u^-$  according to the GRAC functional corresponds to the Rydberg orbital transitions  $3\sigma_{1g} \rightarrow 11\sigma_{2u}(\beta, 45\%)$ ,  $3\sigma_{1g} \rightarrow 4\sigma_{2u}(\alpha, 28\%)$ , and  $2\sigma_{2u} \rightarrow 6\sigma_{1g}(\beta, 4\%)$  and the valence-type orbital transition of  $3\sigma_{1g} \rightarrow 3\sigma_{2u}(\alpha, 15\%)$ . Furthermore, the SAOP functional associates the strong absorption with valence-type orbital transitions of  $3\sigma_{1g} \rightarrow 3\sigma_{2u}(\alpha, 78\%)$  and  $3\sigma_{1g} \rightarrow 3\sigma_{2u}(\beta, 8\%)$  and Rydberg orbital transition of  $3\sigma_{1g} \rightarrow 4\sigma_{2u}(\beta, 8\%)$ . Finally, the strong band calculated by the LB94 functional corresponds to valence-type orbital transitions of  $3\sigma_{1g} \rightarrow 3\sigma_{2u}(\alpha, 48\%)$  and  $3\sigma_{1g} \rightarrow 3\sigma_{2u}(\beta, 24\%)$  and Rydberg orbital transition of  $3\sigma_{1g} \rightarrow 4\sigma_{2u}(\beta, 20\%)$ . It can be seen that the excitation energies of the O<sub>2</sub> molecule calculated by the five different exchange correlation functionals are almost all exceeding the negative HOMO orbital energy (ionization potential) and the excitation energy of the strong band can differ by as much as 2.73 eV with different functionals (e.g., LDAxc and SAOP). Furthermore, the nature of the orbital transitions associated with the strong band is heavily functional dependent. However, as discussed elsewhere<sup>44</sup> excitations with energies exceeding the ionization potential can only be described correctly by asymptotically corrected functionals such as SAOP and LB94 and only the envelope of the ensemble of the peaks has some meaning (individual peaks have no meaning above the ionization threshold).

## CONCLUSION

We have in the present DFT study evaluated ionization potentials for the oxygen molecule both as an energy difference between the neutral molecule and the cation as well as by the HOMO orbital energy using a Koopmans-type DFT theorem. Our study shows that the LDAxc, the B<sub>88</sub>X+P<sub>86</sub>C, and the GRAC exchange correlation functionals affords Koopmans' IPs that are underestimated by about 6.0 eV compared to the energy difference IP and experiment. On the

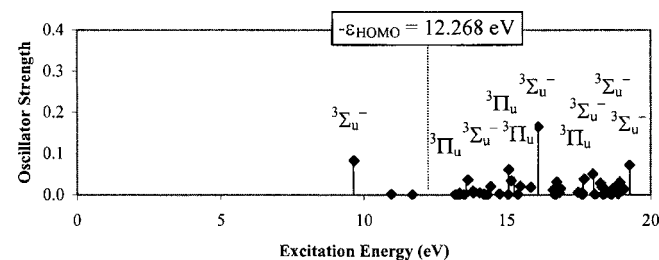


FIG. 5. Excitation spectrum of the oxygen molecule calculated with the SAOP exchange correlation functional.

